AJNR

# Surface coil MR of spinal trauma: preliminary experience.

C B McArdle, M J Crofford, M Mirfakhraee, E G Amparo and J S Calhoun

# Surface Coil MR of Spinal Trauma: Preliminary Experience

Craig B. McArdle[1,2]
Marsha J. Crofford[1]
Mansour Mirfakhraee[1]
Eugenio G. Amparo[1]
Jason S. Calhoun[3]

Nineteen fractured vertebral bodies involving the spine from C1 to L2 in 14 patients were imaged with a 0.6-T magnet using prototypical surface coils. Ten of these patients were studied within the first week of trauma. CT and plain films are superior to MR in detecting fractures and identifying the origin of displaced fragments in cases of extensive comminution. However, all body fractures and most posterior element fractures in the thoracolumbar spine were visible on MR. Fractures involving the cervical neural arch were difficult to detect on transverse section without CT correlation. Our results indicate that MR can probably replace CT in the thoracolumbar region. MR is superior to CT in demonstrating ligamentous injury and trauma to the disk. Unlike CT, MR shows the relation of the thecal sac and spinal cord to retropulsed fragments and epidural hematoma. MR also visualizes cord parenchyma; two cases of cord hemorrhage were not seen on CT. Even at this early stage of development, surface coil MR promises to become important in the evaluation of spinal trauma, not only in assessing the integrity of the spinal canal and cord, but in separating stable from unstable fractures on the basis of disruption of the posterior ligaments and elements. Additionally, the demonstration of rupture of specific ligaments may have an impact on surgical management.

MR of the spine has proven particularly useful in evaluating the spinal cord and degenerative disk disease [1–4]. However, lack of high-resolution, high-signal images obtained from standard body coils has limited the role of MR in imaging the spine. Routine imaging of the spine has been done with sagittal sections. Thin (4- to 5-mm) transverse sections of the spine are not practical without high signal. The relatively low signal-to-noise limitations of the body coil are circumvented by using surface coils. Closely applied to the spine, these coils yield images with two to four times the signal of body coils [5]. Surface coil imaging of lumbar disk disease has been reported, and the results compared favorably with CT [6, 7].

This study records our early experience with surface coil imaging of spinal trauma. We compare our results with plain films and CT, an established technique in evaluating spinal trauma [8–10].

## Materials and Methods

Fourteen patients, aged 16 to 62 years, with 19 fractured vertebral bodies, were imaged with a 0.6-T Technicare superconducting magnet. The distribution of the 19 fractures was as follows: C1 (1), C4 (1), C6 (1), T2 (1), T3 (1), T4 (1), T5 (1), T9 (1), T11 (1), T12 (6), L1 (2), and L2 (2). The predilection for thoracolumbar involvement is once more observed [9, 11]. Elapsed time from injury to MRI ranged from 1 day to 1½ years, with 10 patients imaged within the first week after trauma. We found it preferable to image toward the end of the first week after trauma when the patients were more stable, in less pain, and more able to hold still for the length of the study. This waiting period also improved the likelihood of imaging hemorrhage.

Plain films were available in all cases. CT scans were done in all cases but one (a patient with cervical traction). A GE CT/T 8800 or Siemens DR3 scanner was used to obtain contiguous 5-mm-thick slices with bone and soft-tissue window detail.

## Surface Coils

Three different prototypical surface coils were used in this study: a 13-mm square coil, a 19-cm square coil, and a similarly sized saddle coil. These surface coils only received the signal; the 55-cm body coil acted as the transmitter. The field of view of these surface coils is approximately the diameter of the coil. All patients were imaged supine on the coil. One patient with a C6 fracture was imaged under traction. Our method for MR of the acutely injured patient with cervical traction is described in a separate report [12].

The placement of the flat, square coils was guided by a knowledge of the landmarks shown in Figure 1. Placement was more critical for the small coil and normally required one or two additional manipulations of the coil to center it over the traumatized region. These realignments increased patient discomfort and lengthened the study. The greater imaging diameter of the larger coils improved the ease of coil placement in addition to the quality of the images. (Compare Fig. 3 obtained with a large coil with Fig. 6 obtained with a small coil.) For these reasons, the small coil was abandoned once the larger coils became available in the latter part of this study. The following landmarks were used for centering the larger 19-cm flat coil: thyroid prominence, cervical spine, sternal angle, T1–T6; midsternum, T4–T9; and inferior xyphoid process, T7–L1. The saddle coil provided slightly improved images of the cervical spine over the flat coil because of the wraparound design, minimizing signal fall-off away from the coil.

The acquisition matrix was 256 × 128, giving an in-plane spatial resolution of 0.8 mm in the X axis and 1.6 mm in the Y axis. This is superior to the body coil spatial resolution of 1.6 mm × 3.2 mm.

## Pulse Sequence

A variety of spin-echo (SE) pulse sequences was tried. Imaging time was restricted to 1 hour, about the length of time most patients with acute injuries could tolerate. Centering of the coil over the area of interest was checked by obtaining a short 0.7-min run in the sagittal plane. A single-average SE acquisition with a repetition time (TR) of 300 msec and an echo time (TE) of 38 msec gave five slices. With a 3-mm gap, this acquisition also estimated how off-center from the coil the patient was, side to side. T1- and T2-weighted sagittal and transverse sections were obtained with TRs ranging from 500–2000 msec and TEs of 38–120 msec. For reasons explained in the "Results" section, we preferred the following pulse sequences (TR/TE/number of averages/time of acquisition in min/number of slices): sagittal plane, SE 800/38/4/10.6/17; sagittal plane, SE 1500/38,76/4/13.5/15; transverse plane, SE 500–1000/38/6/6.7–13.5/9–19. Coronal views and moderately T2-weighted transverse sections (SE 1500/60,120) were obtained as needed.

The proton-density-weighted images with SE 1500/38 gave better anatomic detail than the T1-weighted sequence of SE 800/38 because of better signal with longer TR. The T1-weighted sequence helped to confirm hemorrhage. Contiguous slices were obtained with a thickness of 4–5 mm and, as a compromise between signal and time of acquisition,
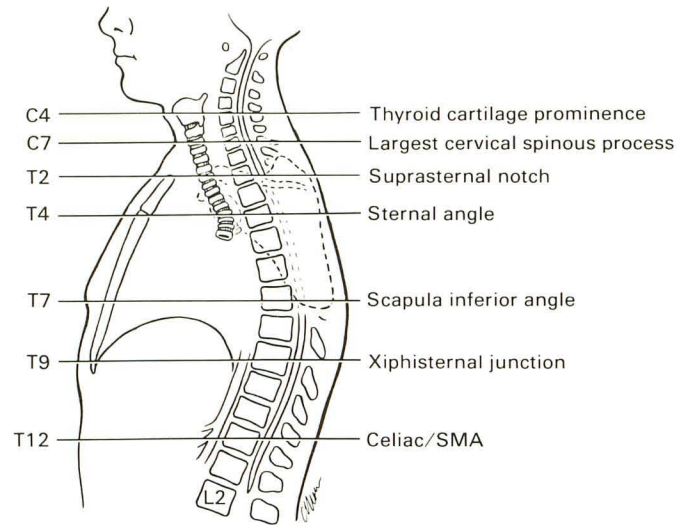


Fig. 1.—Surface coil placement guide. (Adapted from B. Pansky and E. L. House, see reference [13].)

required four averages for the sagittal sections and six averages for the transverse sections. In our experience, obtaining optimal signal is more important than increasing the resolution, since images obtained with high resolution at the expense of signal have decreased contrast. The 90° and 180° tip angles were adjusted for the area of interest and body weight [14].

## Results

### Vertebral Bodies

Contiguous sagittal sections by MR were almost as informative as plain film tomograms and more useful than lateral films of the spine in demonstrating fractures and subluxations (Figs. 2A and 2B). The typical appearance of a flexion-compression fracture was depression of the superior endplate into the body and anterior displacement of fragments and cortex of the crushed body (Figs. 2B and 3B). These fragments were invariably contained by a bulging anterior longitudinal ligament and displayed a medium intensity on T1-weighted scans, becoming darker on the T2-weighted images. However, large fragments with marrow were brighter (Fig. 2B).

Transverse sections by MR through such compression fractures revealed a characteristic pattern (Figs. 2C, 3F, 6A). First, the compressed body had an inhomogeneous signal. Second, the body, typically at the superior endplate, was expanded and bulbous. And third, two or three arcing lines circumscribed the superior aspect of the expanded body. When correlated with CT (Figs. 2D, 3G, 6B), the outermost line represented the anterior longitudinal ligament and/or adherent bony fragments from the body and could be differentiated by the normal, nondisplaced dark cortex because of its wavy, irregular feature. The innermost arcing line correlated with the cortex of the superior endplate driven into the sub-

Fig. 2.—62-year-old woman with bowel and bladder incontinence and mild sensory loss after a T12 compression fracture from a motor vehicle accident 2 weeks before MR study. **A,** Lateral radiograph. Both endplates of T12 are compressed, and bone is displaced anteriorly and posteriorly. **B,** SE 1500/60, same level as in **B.** The mild T2-weighed image clearly displays bulging anterior longitudinal ligament, bone fragments, disk, and fractured endplates. The T11–T12 disk and posteroinferior corner of T12 are bright with hemorrhage. **C,** SE 1500/60, superior T12 level. Two peripheral arcing black lines circumscribe the expanded body (*black arrows*). A third, fainter, inner dark line is evident (*white arrow*). Also note curvilinear white line (*arrowhead*). **D,** CT at approximately same level explains origin of lines in **C.** See text for further description. **E,** SE 1500/60, mid-T12 level. Faint dark and light lines in body indicate fractures. Note abnormal orientation of right facet joint and misshapen right T11 inferior process (*arrowhead*). Retropulsed bone compresses thecal sac and flattens cord. **F,** CT scan at level of **F.** Fractures are better seen. Spinal canal detail is poor, and there is no way to estimate from extent of canal narrowing the degree to which cord is impinged upon.
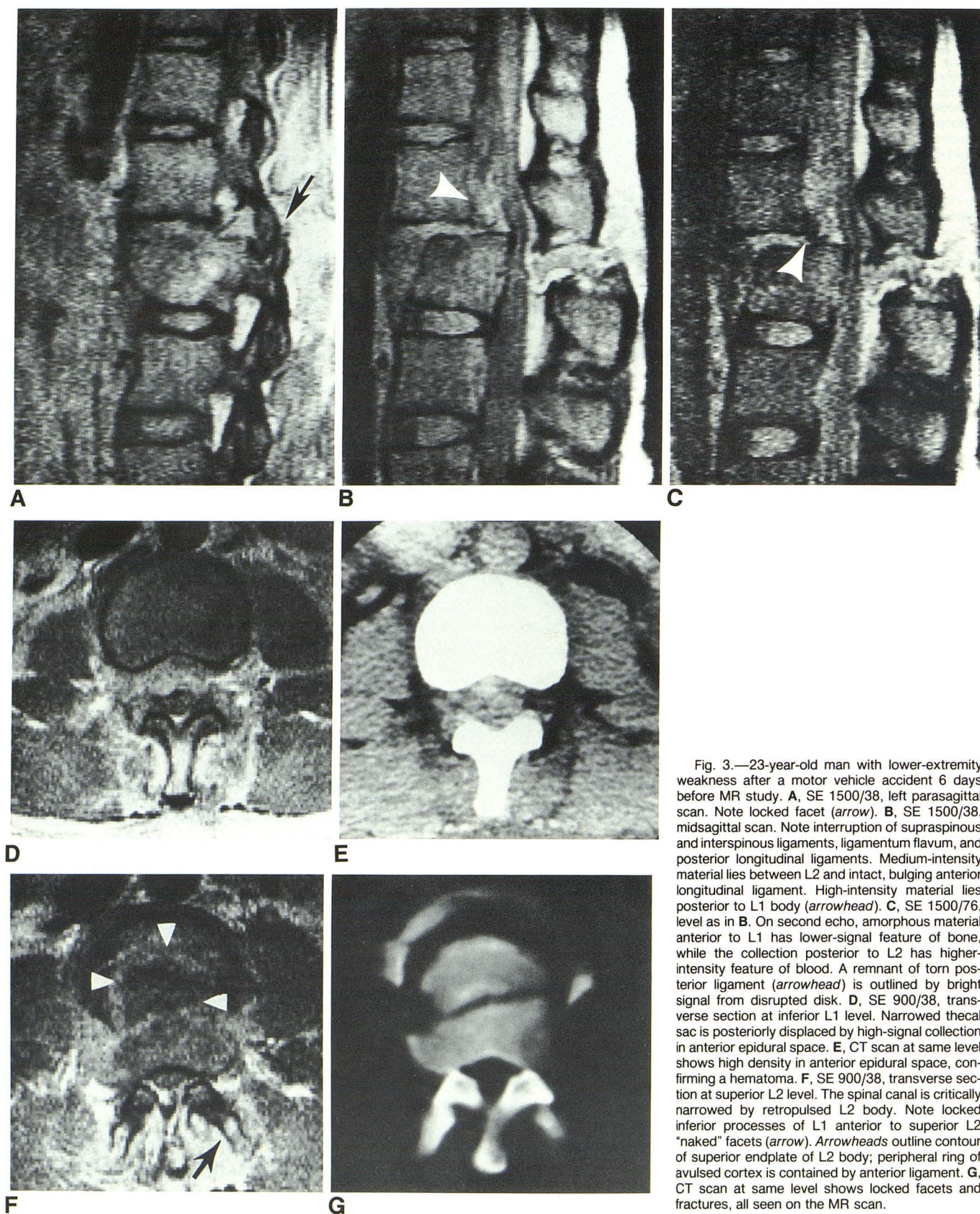
A

B

C

D

E

F
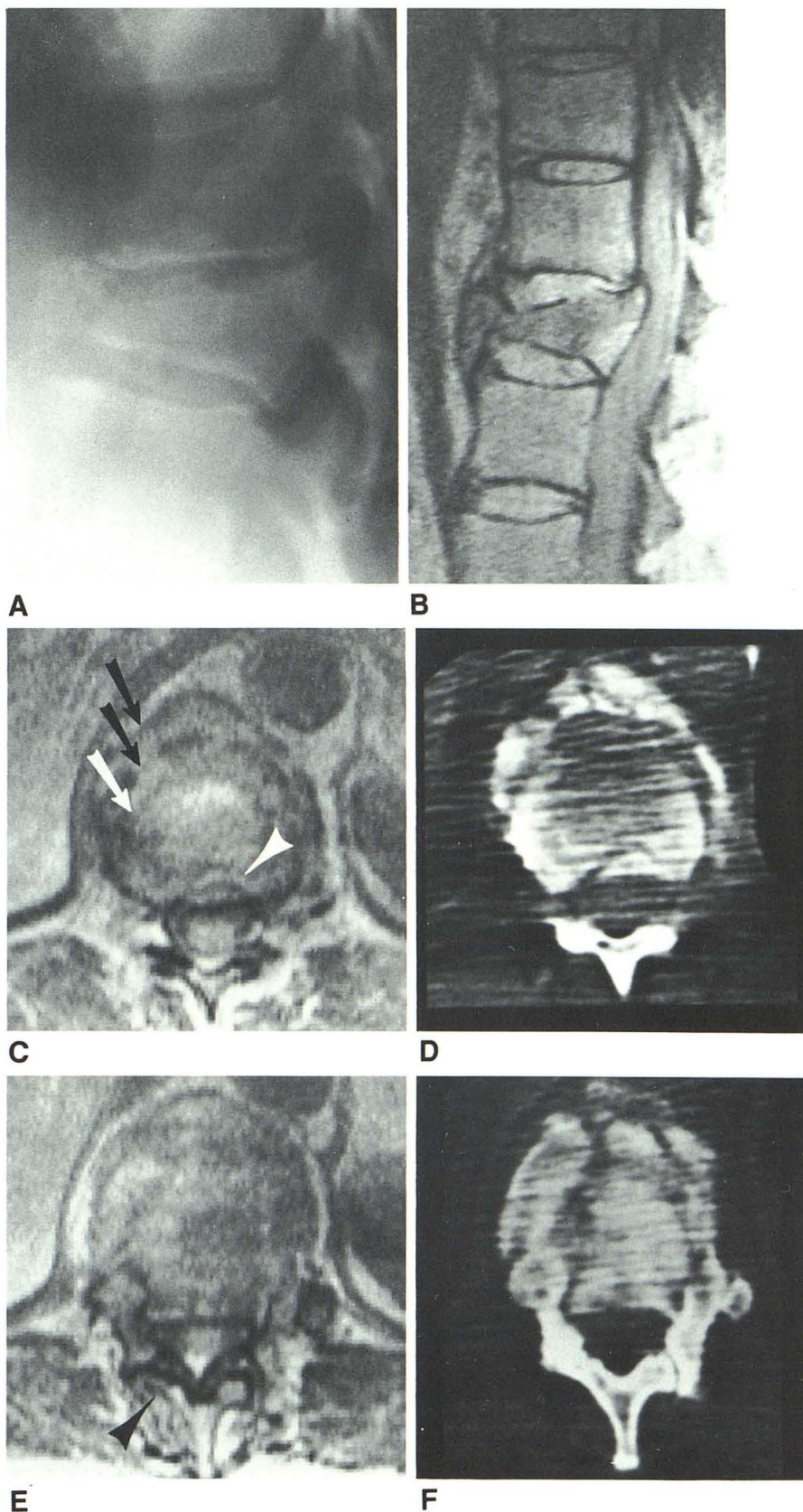
Fig. 3.—23-year-old man with lower-extremity weakness after a motor vehicle accident 6 days before MR study. **A**, SE 1500/38, left parasagittal scan. Note locked facet (*arrow*). **B**, SE 1500/38, midsagittal scan. Note interruption of supraspinous and interspinous ligaments, ligamentum flavum, and posterior longitudinal ligaments. Medium-intensity material lies between L2 and intact, bulging anterior longitudinal ligament. High-intensity material lies posterior to L1 body (*arrowhead*). **C**, SE 1500/76, level as in **B**. On second echo, amorphous material anterior to L1 has lower-signal feature of bone, while the collection posterior to L2 has higher-intensity feature of blood. A remnant of torn posterior ligament (*arrowhead*) is outlined by bright signal from disrupted disk. **D**, SE 900/38, transverse section at inferior L1 level. Narrowed thecal sac is posteriorly displaced by high-signal collection in anterior epidural space. **E**, CT scan at same level shows high density in anterior epidural space, confirming a hematoma. **F**, SE 900/38, transverse section at superior L2 level. The spinal canal is critically narrowed by retropulsed L2 body. Note locked inferior processes of L1 anterior to superior L2 "naked" facets (*arrow*). *Arrowheads* outline contour of superior endplate of L2 body; peripheral ring of avulsed cortex is contained by anterior ligament. **G**, CT scan at same level shows locked facets and fractures, all seen on the MR scan.

Fig. 4.—43-year-old woman with complete paraplegia after compression fractures of T11 and T12; imaged 3 days after trauma. **A**, SE 1000/38, inferior T11 level. Thecal sac is displaced to right by an intermediate-signal mass (*arrow*). The spinal cord has increased signal. **B**, CT scan at level of **D**. Intermediate-signal mass is a bony fragment from T11 body. **C**, SE 1000/38, T11–T12 disk level. Spinal canal is markedly narrowed by intermediate signal mass continuous with the disk. Spinal cord appears as a bright slit (*arrowhead*). Normal facet joints at level of inferior articulating process of T11 are not seen. **D**, CT scan at above level. Disk herniates into spinal canal. Right facet joint is distracted; left joint is disarticulated.

A

B

C

D
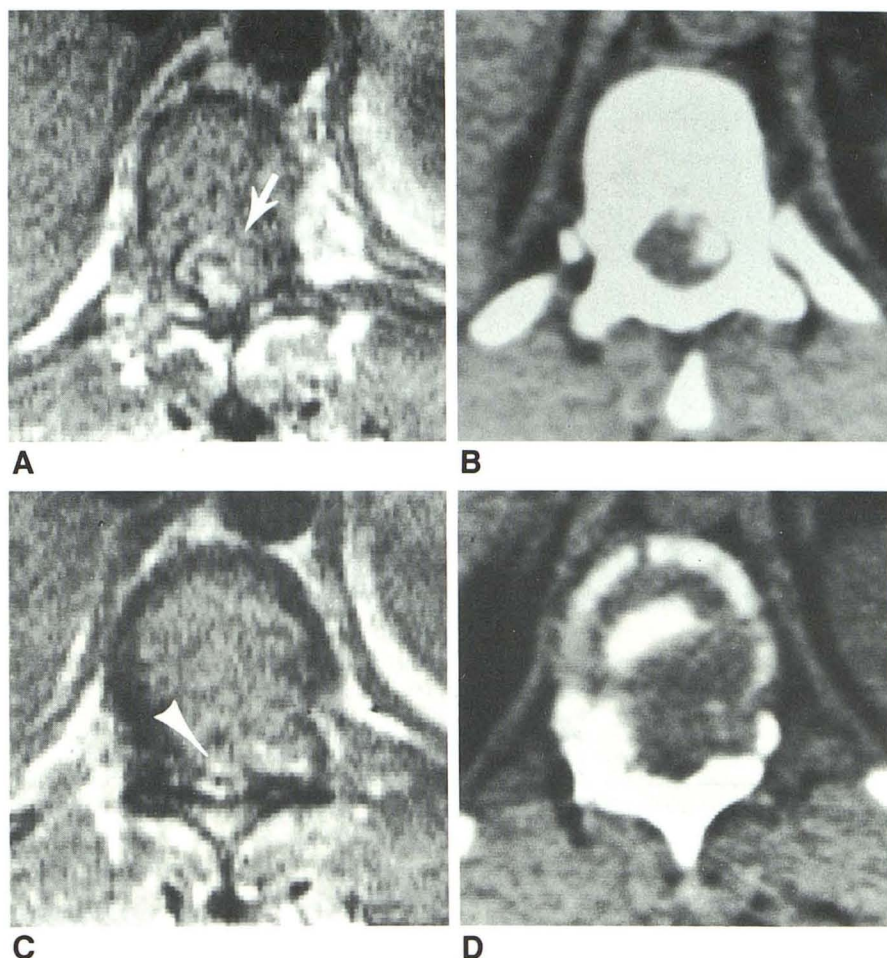
stance of the body. Occasionally, a third line could be seen between these two lines if the endplate cortex was avulsed and separated from the endplate margin (Fig. 2D).

In nine of 10 acutely fractured vertebral bodies, the body had increased signal compared with adjacent bodies on T2-weighted sequences (Figs. 2B, 5C). This was most obvious on the sagittal view. Less intense but still increased signal was apparent on proton-density-weighted sequences with a TR of 1500 msec and a TE of 38 msec. The T1-weighted images showed mild increase in signal in those fractures imaged at least 6 days after trauma, but no difference in intensity was noticed in those fractures imaged 1–4 days after trauma.

Significant fractures of the body were seen on both MR and CT, but these fractures were easier to see on CT (Figs. 2E and 2F). Detecting these fractures on MR was more difficult. Fracture lines appeared either dark or light, relative to adjacent marrow and cortical endplate. Fractures with signal were noted as early as 2 days after trauma. Fractures through marrow tended to be less sharply defined and more poorly outlined by the signal inhomogeneity of the comminuted body (Figs. 2E and 3F). Fractures through the cortex

were the easiest to read, since these fractures resembled those on CT. The fracture lines were sharply defined and ran perpendicular to the cortex, and were often associated with cortical malalignment.

Fractures were best seen on the T1-weighted or proton-density-weighted images. As the TR was increased from 500 to 1500 msec, the marrow became brighter. Dark fractures stood out, and light fractures were more intense than the marrow. As the TE was increased from 38 to 120 msec, the marrow and fractures also became brighter, but the loss of signal rendered the images noisy, and subtle fractures could be more easily missed on transverse sections.

*Posterior Elements*

Trauma to the posterior elements was found in nine of 14 cases. In all cases, neural arch fractures or facet disarticulation were apparent on the MR scan and, in the thoracolumbar spine, showed very good correlation with CT (Figs. 2E, 2F, 3F, 3G, 4C, 4D). Sagittal sections were helpful in demonstrating locked or perched facets at all levels, including the cervical

**A**                                        **B**                                        **C**
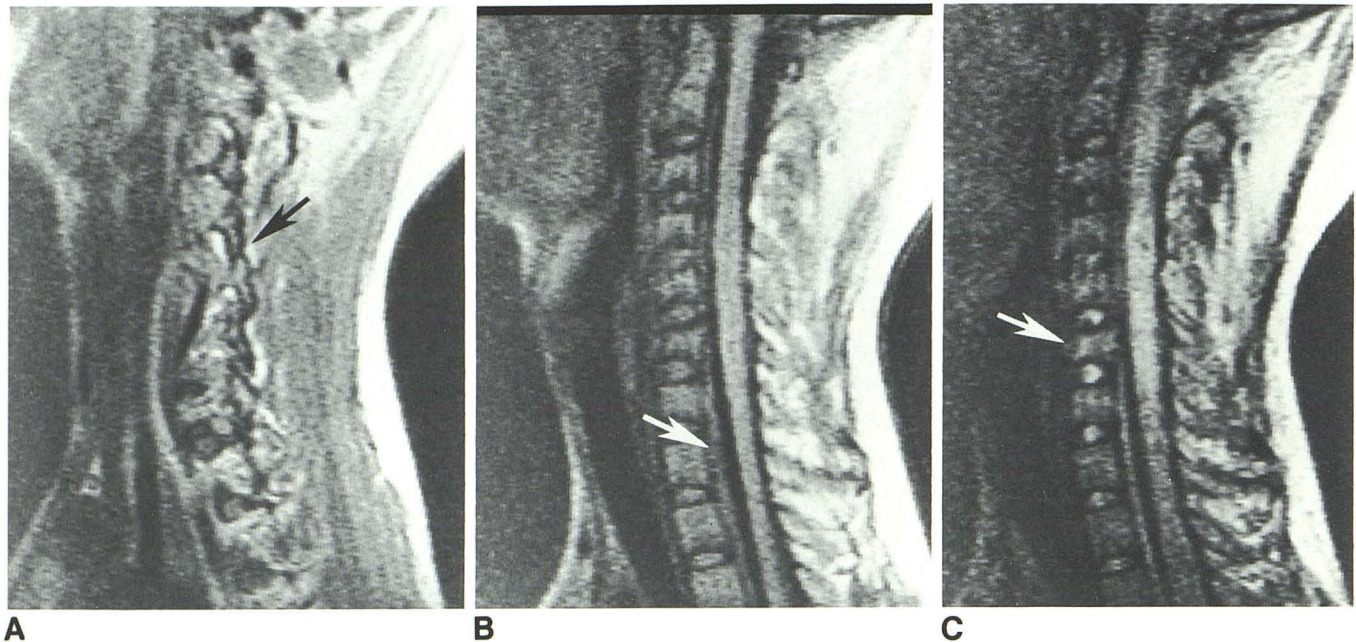
Fig. 5.—16-year-old boy with complete quadriplegia after a motor vehicle accident 4 days before MR study. Patient is imaged with 35 lbs (15.9 kg) of cervical traction. **A**, SE 1500/38, left parasagittal scan. Note locked facet with anterior slippage of C4 inferior process with respect to C5 (*arrow*) and nearly perched facet at C5–C6. **B**, SE 700/38, midsagittal scan. Midcervical cord is fusiformly enlarged and bright. Linear area of increased signal below C6 compressed body (*arrow*) underlies posterior longitudinal ligament. Thin line posterior to superior bodies is normal epidural fat. Traction accounts for straightened cervical spine and widened disk spaces. **C**, SE 1500/76. On this T2-weighted scan, the abnormal areas of increased signal in cord and posterior bodies intensify; and together with T1-weighted scan, indicate hemorrhage. Compressed C6 body (*arrow*) has somewhat higher signal than other vertebral bodies.

spine (Figs. 3A, 5A).

Although the posterior elements do not contain much marrow, in the thoracolumbar spine their dark cortices and closely opposed ligamentum flava are well outlined anteriorly by epidural fat and posteriorly by fat separating them from the adjacent paraspinous muscles. Fractures and asymmetry in the orientation of the posterior elements were easy to see. On the other hand, fractures of the posterior elements of the cervical spine were difficult to visualize on transverse sections without the CT scan for comparison, because these small, thin bones are not surrounded by much fat.

### Disks

The increased signal imparted to disks on T2-weighted images makes this pulse sequence ideal for evaluating trauma to the disk and structures adjacent to it. Endplate fractures were better seen, as were tears of the anterior and posterior longitudinal ligaments (Figs. 2B, 3C). Altered disk morphology and signal were observed in three cases. A more intense signal to the disk was associated with comminution of the superior endplate in one case (Fig. 2B). Disk herniated into the spinal canal in two cases, associated with rupture of the posterior longitudinal ligament.

### Ligaments

Rupture of the supportive ligaments of the spine was not uncommon in our series; it was seen in five of nine cases of the thoracolumbar spine imaged within the first week of trauma (Figs. 3B and 3C). Tears of the longitudinal, ligamentum flavum, interspinous, and supraspinous ligaments were all best evaluated on the sagittal view. The supraspinous ligament appeared as a dark stripe overlying the tips of the spinous processes and was well outlined by the subcutaneous fat posteriorly. The interspinous ligaments appeared as a low intensity band filling in the space between the spinous processes. All five cases of posterior ligament tears were associated with significant posterior element fractures and/or disarticulation.

### Spinal Canal and Cord

MR was most useful in evaluating the spinal canal and cord. Both CT and MR demonstrated fragments impinging on the canal, but only MR showed the relation of the thecal sac and cord to these retropulsed fragments (Figs. 2E, 2F, 3F, 3G, 4A–D). Sagittal views provided an overview of the traumatized region, but 4- to 5-mm thin transverse sections were critical for a thorough study. Transverse cuts imaged the whole canal and accurately depicted any displacement of the thecal sac. T1-weighted sequences best demonstrated the low-intensity CSF, contrasting with the bright epidural fat.

On transverse T1-weighted images, distinction between retropulsed bony fragments and disk material was difficult, since both appeared as medium-intensity structures (Figs. 4A and 4C). However, the sagittal view showed the origin of the retropulsed fragment or herniated disk. T2-weighted trans-

Fig. 6.—44-year-old man with new progressive lower-limb weakness and sensory loss 1½ years after sustaining T9 and T12 compression fractures. **A**, SE 900/38, superior T12 level. Signs of endplate compression are present, including inhomogeneous signal to the expanded body and arcing inner dark line. Flattened spinal cord is pinched between abnormally convex posterior body and left lamina (*arrowhead*). **B**, CT scan at same level shows spinal canal narrowing. Position of cord cannot be ascertained. Comminuted vertebral body is confirmed.
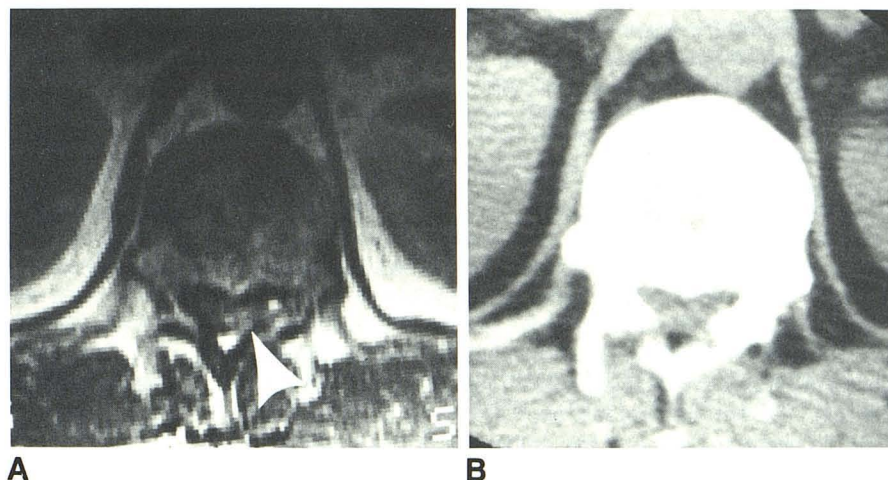
verse scans were also useful: disk material was more intense than marrow.

There were two cases of epidural hematoma confirmed by CT, and two suspected cases. In one case, 3 days after trauma, non-T2-weighted transverse sections revealed a collection with the low-intermediate intensity of bone fragment but lacking its sharp margins. In another case, 6 days after trauma, the collection had a higher signal but still less than epidural fat (Figs. 3B–E). In all cases, confirmed and suspected, T2-weighted sections increased the intensity of the hematoma to about the same or slightly lower intensity as that of the fat.

On T1-weighted or proton-density-weighted pulse sequences, the CSF was dark and the higher signal cord was well seen. The lower intensity central gray matter of the cord was often distinguished from the peripheral white matter (Fig. 5B). Cord hemorrhage, presenting as increased signal on non-T2-weighted sequences, was punctate in one case, involved a focal segment in another (Figs. 4A and 4C), and was diffuse in a third (Figs. 5B and 5C). In the latter two cases, the patients were paralyzed. CT did not reveal cord densities in the first two cases (the third patient did not have a CT).

## Discussion

Use of the surface coil and thin sections yields images containing a wealth of information. The information combines many of the best features of conventional tomography, CT, and myelography. Like tomography, MR offers the ease of obtaining slices in sagittal and coronal planes but without the inconvenience of moving the patient. The MR plane is not localized to the immediate area of trauma, as with CT reconstruction. MR also provides the cross-sectional information of CT and detects clinically significant fractures of the thoracolumbar spine. MR is at least as good as myelography in visualizing the thecal sac and cord contour, and it surpasses CT myelography in its depiction of cord parenchyma.

Compared with CT, MR better demonstrates the intervertebral disk. MR also directly images the supporting ligaments of the spine; previously, damage to these ligaments could only be inferred by CT. MR is also superior to CT in displaying the spinal canal. Previous studies have failed to show any correlation between the degree of canal narrowing by retropulsed fragments and the extent of neurologic injury [15, 16]. Figures 2F and 6B show there is no way to predict the location of the spinal cord on CT in cases where the spinal canal is not critically narrowed.

Nonacute (>1 week) hemorrhage is more easily seen by MR than CT and is the most likely explanation for the increased signal on the T1-weighted and proton-density-weighted images in the vertebral bodies, the fracture lines, the ruptured disks, and areas within the cord. The increased vertebral body signal was seen only in those fractures with comminution of the endplates, probably owing to fracture extension into the basivertebral venous channels.

CT visualizes hemorrhage earlier than does MR [17]. However, MR visualizes hemorrhage longer, since methemoglobin is slowly resorbed, and the intensity of the blood collections may persist for weeks or months [18]. Hemorrhage on MR becomes easier to detect toward the end of the first week and is one reason to delay imaging spinal trauma beyond the first few days. Epidural hematoma should be most obvious within the first week, when its lack of intensity contrasts more with the bright epidural fat. Once the hematoma ages and the hemorrhage intensity increases, the mass effect may persist, but the increased signal from the hemorrhage may be masked by the fat. This masking has been reported for retrobulbar hemorrhage in periorbital fat [19] and in our experience with MR of orbital blow-out fractures [20].

We were encouraged by the MR demonstration of thoracolumbar body and posterior element fractures. However, we were in all cases aided by CT studies, which facilitated our interpretation. CT is superior to MR in imaging fractures and identifying fragments in cases of extensive posterior element comminution or fracture-dislocation. Nevertheless, we feel that with experience, significant fractures of the thoracolumbar spine can be detected, especially if sagittal and transverse sections are used.

Compared with its use in the thoracolumbar spine, MR may play a more limited role in evaluating cervical fractures. The small bones and little fat surrounding the neural arches make it difficult to directly visualize fractures of the posterior ele-

ments. This is a problem that is also shared with CT [21]. Sagittal and coronal views infer the presence of fractures. Nevertheless, for the present MR will still play an important role in assessing the status of the cervical spinal canal and cord.

That MR misses some fractures that CT shows may not be important in patient management. Since Holdsworth's original classification of spinal trauma [22] there have been many attempts at categorizing fractures on the basis of their appearance to determine whether the fracture is stable or unstable [15, 23–25]. More recently, less emphasis has been placed on fracture description because of overlap in categories, so that some stable wedge fractures under one classification system are unstable even if there is no dislocation [26]. To overcome some of this ambiguity, newer systems of classification place more emphasis on the integrity of the ligamentous support of the spine [15, 25]. Tears of the posterior longitudinal ligament, ligamentum flavum, interspinous and supraspinous ligaments, and facet joint disruption are viewed as potentially unstable [15]. The type of injury also determines the surgical procedure, whether to use compressive or distractive Harrington rods or segmental spinal instrumentation [15]. Demonstrating rupture of specific ligaments would be of value. For example, Harrington distractive rods, indicated in fractures with retropulsed fragments, would not be used if the anterior ligament was torn [25]. The presence of these injuries is only deduced on CT from displaced fragments and fractures, but MR can directly visualize these ligaments.

MR is capable of showing subtle abnormalities in the epidural space with concurrent thecal sac deformity. However, identifying the cause of the mass effect can be a problem. On T1-weighted transverse scans, it may not always be possible to distinguish between bony fragments, herniated disk material, and acute epidural hematomas, since all have medium-intensity signal relative to fat. Further experience may define criteria to allow distinction. We found sagittal sections and selective use of T2-weighted transverse sections helpful in separating retropulsed bony fragments from herniated disks.

Our results show that surface coil MR promises to become increasingly important in evaluating spinal trauma. MR can probably replace CT in the thoracolumbar region. Good quality anteroposterior and lateral plain films should always be obtained to determine which vertebral bodies are involved, since surface coil MR limits the field of view. MR can then be performed with contiguous 4- to 5-mm thin sections in sagittal and transverse planes; coronal sections may be helpful below and including T12, where the facet joints assume a more sagittal orientation. Limited CT can be done if it is important to determine the cause of epidural mass effect or in cases of extensive comminution and disorientation of the posterior elements, which may require the improved contrast of bone on CT to identify their origin. We see no role for myelography or conventional tomography if the MR study is optimal.

Further refinement in technique should reduce the number of signal averages required to obtain satisfactory images, thereby shortening the total examination time. With improved coil and gradient design, thin sections can be obtained with less signal averaging. Part of the saved time can be used to increase the number of matrix elements in the Y axis without sacrificing signal, increasing the resolution and making it easier to detect more subtle fractures of the posterior elements. Even at this stage of development, the information derived from the MR study more than makes up for the examination time, considering that CT, intrathecal contrast, and, occasionally, conventional tomography are needed to provide much of the same information.

## REFERENCES

1. Norman D, Mills CM, Brant-Zawadzki M, Yeates A, Crooks LE, Kaufman L. Magnetic resonance imaging of the spinal cord and canal: potentials and limitations. *AJR* **1983**;141:1147–1152, *AJNR* **1984**;5:9–14
2. Modic MT, Pavlicek W, Weinstein MA, et al. Magnetic resonance imaging of intervertebral disk disease. *Radiology* **1984**;152:103–111
3. Hyman RA, Edwards JH, Vacirca SJ, Stein HL. 0.6T MR imaging of the cervical spine: multislice and multiecho techniques. *AJNR* **1985**;6:229–236
4. Cammoun D, Seibert C, Morgan C, Smazal S, Edgar R, Schiffer L. Magnetic resonance imaging (MRI) of the spine and spinal cord. Abstract. *Mag Res Imag* **1985**;3:182
5. Edelman RR, McFarland E, Stark DD, et al. Surface coil MR imaging of abdominal viscera. Part I. Theory, technique, and initial results. *Radiology* **1985**;157:425–430
6. Edelman RR, Shoukimas GM, Stark DD, et al. High-resolution surface-coil imaging of lumbar disk disease. *AJNR* **1985**;6:479–485, *AJR* **1985**;144:1123–1129
7. Maravilla KR, Sory C, Lesh P, Weinreb JC. Magnetic resonance imaging techniques for evaluation of the lumbar spine. Abstract. *Mag Res Imag* **1985**;3:182
8. Handel SF, Lee Y-Y. Computed tomography of spinal fractures. *Radiol Clin North Am* **1981**;19:69–89
9. Brant-Zawadzki M, Jeffrey RB Jr, Miragi H, Pitts LH. High resolution CT of thoracolumbar fractures. *AJNR* **1982**;3:69–74, *AJR* **1982**;138:699–704
10. Post MJD, Green BA. Use of computed tomography in spinal trauma. *Radiol Clin North Am* **1983**;21:327–375
11. Kilcoyne RF, Mack LA, King HA, Ratcliffe SS, Loop JW. Thoracolumbar spine injuries associated with vertical plunges: reappraisal with computed tomography. *Radiology* **1983**;146:137–140
12. McArdle CB, Wright JW, Prevost WJ, Dornfest DJ, Amparo EG. MR imaging of the acutely injured patient with cervical traction. *Radiology* **1986**;159:273–274
13. Pansky B, House EL. *Review of gross anatomy*, 3d ed., New York: Macmillan, **1975**:148
14. Kneeland JB, Knowles RJR, Cahill PT. Magnetic resonance imaging systems: optimization in clinical use. *Radiology* **1984**;153:473–478

15. McAfee PC, Yuan HA, Fredrickson BE, Lubicky JP. The value of computed tomography in thoracolumbar fractures. *J Bone Joint Surg (Am)* **1983**;65:461–473

16. Shuman WP, Rogers JV, Sickler ME, et al. Thoracolumbar burst fractures: CT dimensions of the spinal canal relative to post-surgical improvement. *AJNR* **1985**;6:337–341, *AJR* **1985**; 145:337–341

17. Bradley WG Jr, Schmidt PG. Effect of methemoglobin formation on the MR appearance of subarachnoid hemorrage. *Radiology* **1985**;156:99–103

18. Gomori JM, Grossman RI, Goldberg HI, Zimmerman RA, Bilaniuk LT. Intracranial hematomas: imaging by high-field MR. *Radiology* **1985**;157:87–93

19. Edwards JH, Hyman RA, Vacirca SJ, et al. 0.6 T magnetic resonance imaging of the orbit. *AJNR* **1985**;6:253–258, *AJR* **1985**;144:1015–1020

20. McArdle CB, Amparo EG, Mirfakhraee M. MR imaging of orbital blow-out fractures. *J Comput Assist Tomogr* **1986**;10:116–119

21. Pech P, Kilgore DP, Pojunas KW, Haughton VM. Cervical spinal fractures: CT detection. *Radiology* **1985**;157:117–120

22. Holdsworth F. Fractures, dislocations, and fracture-dislocations of the spine. *J Bone Joint Surg* **1970**;52(A):1534–1551

23. Lindahl S, Willen J, Nordwall A, Irstam L. The crush-cleavage fracture: a "new" thoracolumbar unstable fracture. *Spine* **1983**;8:559–569

24. Denis F. Updated classification of thoracolumbar fractures. *Orthop Trans* **1982**;6:8–9

25. Ferguson RL, Allen BL Jr. A mechanistic classification of thoracolumbar spine fractures. *Clin Orthop* **1984**;189:77–88

26. Jelsma RK, Kirsch PT, Rice JF, Jelsma LF. The radiologic description of thoracolumbar fractures. *Surg Neurol* **1982**;18:230–236